The Astronomical Journal, 155:248 (16pp), 2018 June https://doi.org/10.3847/1538-3881/aac0ff

The Plutino Population: An Abundance of Contact Binaries

Audrey Thirouin[1] and Scott S. Sheppard[2]
[1] Lowell Observatory, 1400 W Mars Hill Road, Flagstaff, AZ 86001, USA; thirouin@lowell.edu
[2] Department of Terrestrial Magnetism (DTM), Carnegie Institution for Science, 5241 Broad Branch Road NW, Washington, District of Columbia, 20015, USA
ssheppard@carnegiescience.edu
Received 2017 December 16; revised 2018 March 27; accepted 2018 April 25; published 2018 May 24

Abstract

We observed 12 Plutinos over two separated years with the 4.3 m Lowell's Discovery Channel Telescope. Here, we present the first light-curve data for those objects. Three of them (2014 JL_{80}, 2014 JO_{80}, and 2014 JQ_{80}) display a large light-curve amplitude explainable by a single elongated object, but they are most likely caused by a contact binary system due to their light-curve morphology. These potential contact binaries have rotational periods from 6.3 to 34.9 hr and peak-to-peak light-curve variability between 0.6 and 0.8 mag. We present partial light curves, allowing us to constrain the light-curve amplitude and the rotational period of another nine Plutinos. By merging our data with the literature, we estimate that up to ∼40% of the Plutinos could be contact binaries. Interestingly, we found that all of the suspected contact binaries in the 3:2 resonance are small with absolute magnitude $H > 6$ mag. Based on our sample and the literature, up to ∼50% of the small Plutinos are potential contact binaries.

Key words: Kuiper belt objects: individual (2014 JL80, 2014 JO80, 2014 JQ80) – techniques: photometric

1. Introduction

Any object confined in a mean motion resonance with Neptune receives the name "*resonant object*". At ∼39.4 au, the 2:3 resonance is the most stable and densely populated resonance (Jewitt et al. 1998; Chiang & Jordan 2002). As Pluto is a 3:2 resonant object, all bodies trapped into this resonance receive the denomination of *Plutinos*. According to Malhotra (1995), some Plutinos cross Neptune's orbit, but they never suffer a close approach. The overabundance of Plutinos is likely due to Neptune's migration (Malhotra 1993, 1995). Neptune could have been created in the inner solar system and migrated outwards to its actual location, due to angular momentum exchange with surrounding planetesimals (Fernandez & Ip 1984). With Neptune's migration, the resonances moved into the trans-Neptunian belt, and the planetesimals were captured by such resonances (Malhotra 1995; Levison et al. 2008). Thus, the migration and circularization of this planet's orbit provoked the capture of objects into the resonances. A migration of ∼8 au over 10^7 years reproduces the observed distribution of Plutinos (Gomes 2000).

Several of the largest Plutinos are binaries or multiple systems: Pluto–Charon (and four smaller moons), Huya (formerly 2000 EB_{173}), Orcus–Vanth (2004 DW), Lempo (1999 TC_{36}, triple system), and 2003 AZ_{84}. These binaries are likely formed by collisional impact on the primary. Trapped in the Plutinos, Mors–Somnus (2007 TY_{430}) is a noteworthy equal-sized wide system that cannot have been created by impact and is like a dynamically Cold Classical equal-sized binary (Sheppard et al. 2012). Finally, 2001 QG_{298} is a near equal-sized contact binary (Sheppard & Jewitt 2004). Therefore, less than 3% of the Plutinos are known binaries. The Plutino population seems to have a deficit in separated wide binary systems compared to the other dynamical groups (Noll et al. 2008; Compère et al. 2013). As said in Thirouin et al. (2017), contact binaries are unresolved with the *Hubble Space Telescope (HST)*. These compact systems may remain undiscovered, and therefore the current fraction of close/compact binary systems in the Plutino population and other populations by extension are unknown. Similarly, as argued by Porter & Grundy (2012), there is potentially a large fraction of binaries with circular and very tight orbits due to Kozai effects that are undetectable with *HST*. Even if it remains unclear how contact binaries are formed, one can argue that tidal effects as suggested by Porter & Grundy (2012) can create very tight orbits (but note that the gravitational collapse is also an option; Nesvorný et al. 2010). Finally, as suggested by the star formation theory, if a triple system looses one component, the other two objects have to shrink their orbit to go back to a stable configuration and can potentially create a contact/close binary (Bodenheimer 2011). However, it is important to point out that several of theses models are not dedicated to the TNO science and that we are still missing several observables to infer if a model is working or not. It is our hope that our work on contact binaries will help to constrain their localizations, characteristics, and fraction, among other properties, which can be used for modeling or as observables to check the validity of a model.

2. Data Reduction, Analysis, and Results

Data obtained between 2017 May and July, and 2015 November–December with the Lowell Observatory's 4.3 m Discovery Channel Telescope (DCT) are presented. We used exposure times of 300–500 s with a broad-band filter with the Large Monolithic Imager (LMI) (Levine et al. 2012). Details about the telescope and instrument can be found in Thirouin et al. (2017). The observing log is in Table 1.

The data reduction and analysis are the same as in our previous works, the main steps of which are summarized as follows. Images were biased subtracted and flatfielded thanks to calibration images obtained each night (dome and/or twilight flats depending on the weather conditions). Then, we proceed with the aperture photometry with a data reduction software using the Daophot routines described in Stetson (1987). The optimal aperture radius in order to estimate the flux of the object and limit the background contamination has been estimated by a growth curve (Howell 1989; Stetson 1990). We selected 20 stars per field as reference stars. We also played with the pointings in order to keep about the same field of view

Table 1
UT-dates, Heliocentric and Geocentric (r_h, Δ, respectively) Distances, and Phase Angle (α, in degrees) Are Summarized

Object	UT-date	Nb. of Images	r_h (au)	Δ (au)	α (°)	Filter	Telescope
1995 HM_5							
	2017 May 20	9	29.656	28.647	0.2	VR	DCT
(469362) 2001 KB_{77}							
	2017 Jun 18	6	28.731	27.750	0.5	VR	DCT
2006 UZ_{184}							
	2015 Nov 30	6	31.029	30.076–30.077	0.5	VR	DCT
	2015 Dec 01	4	31.030	30.082	0.5	VR	DCT
2014 JL_{80}							
	2017 May 28	10	28.563	27.578	0.5	VR	DCT
	2017 May 29	18	28.563	27.581–27.582	0.5	VR	DCT
	2017 Jun 18	7	28.559	27.706–27.707	1.1	VR	DCT
	2017 Jun 28	6	28.557	27.806–27.807	1.4	VR	DCT
2014 JK_{80}							
	2017 Jun 27	4	35.236	34.446–34.447	1.1	VR	DCT
	2017 Jun 28	6	35.235	34.454–34.455	1.1	VR	DCT
2014 JO_{80}							
	2017 Jun 18	13	31.938–31.939	31.008–31.009	0.7	VR	DCT
	2017 Jun 27	4	31.945	31.078–31.079	1.0	VR	DCT
	2017 Jun 28	12	31.946	31.086–31.087	1.0	VR	DCT
	2017 Jul 02	13	31.949	31.124–31.126	1.1	VR	DCT
2014 JP_{80}							
	2017 Jun 27	5	42.207	41.349	0.7	VR	DCT
2014 JQ_{80}							
	2017 May 01	23	31.627	30.670–30.669	0.6	VR	DCT
	2017 May 20	17	31.633	30.627–30.628	0.2	VR	DCT
	2017 May 28	20	31.635	30.641–30.642	0.4	VR	DCT
	2017 May 29	10	31.636	30.644–30.645	0.4	VR	DCT
	2017 Jun 18	7	31.642	30.762–30.764	0.9	VR	DCT
	2017 Jun 27	6	31.645	30.850–30.851	1.2	VR	DCT
2014 JT_{80}							
	2017 Jun 27	5	32.245	31.302–31.303	0.7	VR	DCT
2014 KC_{102}							
	2017 Jun 18	4	30.505	29.526	0.5	VR	DCT
	2017 Jul 02	15	30.498	29.581–29.582	0.8	VR	DCT
2014 KX_{101}							
	2017 May 28	12	31.153	30.143	0.1	VR	DCT
	2017 May 29	5	31.154	30.142	0.1	VR	DCT
2015 BA_{519}							
	2017 May 01	16	31.041	30.053	0.4	VR	DCT

every night and thus the same reference stars or at least keep a couple of reference stars in common between pointings. Such a technique allows us to use the same reference stars across observing runs and also allow us to merge our data sets. The error associated with the photometry has been estimated following the formalism in Howell (1989). Finally, we looked for periodicities using the Lomb periodogram technique (Lomb 1976; Press et al. 1992) and double-checked our results with the Phase Dispersion Minimization from Stellingwerf (1978). Additional details about our data reduction/analysis procedures are available in Thirouin et al. (2010, 2012), Thirouin (2013).

In this section, we present our photometric results for our partial and complete light curves. All of our light curves with a rotational period estimate are plotted over two cycles. In the case of a partial light curve without a rotational period estimate, the photometry with error bars is plotted versus Julian Date (no light-time correction applied). We summarize our photometry in the Appendix, and our results are reported in Table 2.

It is important to point out that our study was designed to constrain the percentage of large-amplitude objects in the Plutino population. Therefore, if an object was not showing obvious signs of large variability that is characteristic of a contact binary, we stop observing it. But, in some cases, our observations were interrupted due to bad weather and/or smoke. In conclusion, for the rest of our study, all objects with an observed variability smaller than 0.2 mag will be considered as noncontact binaries.

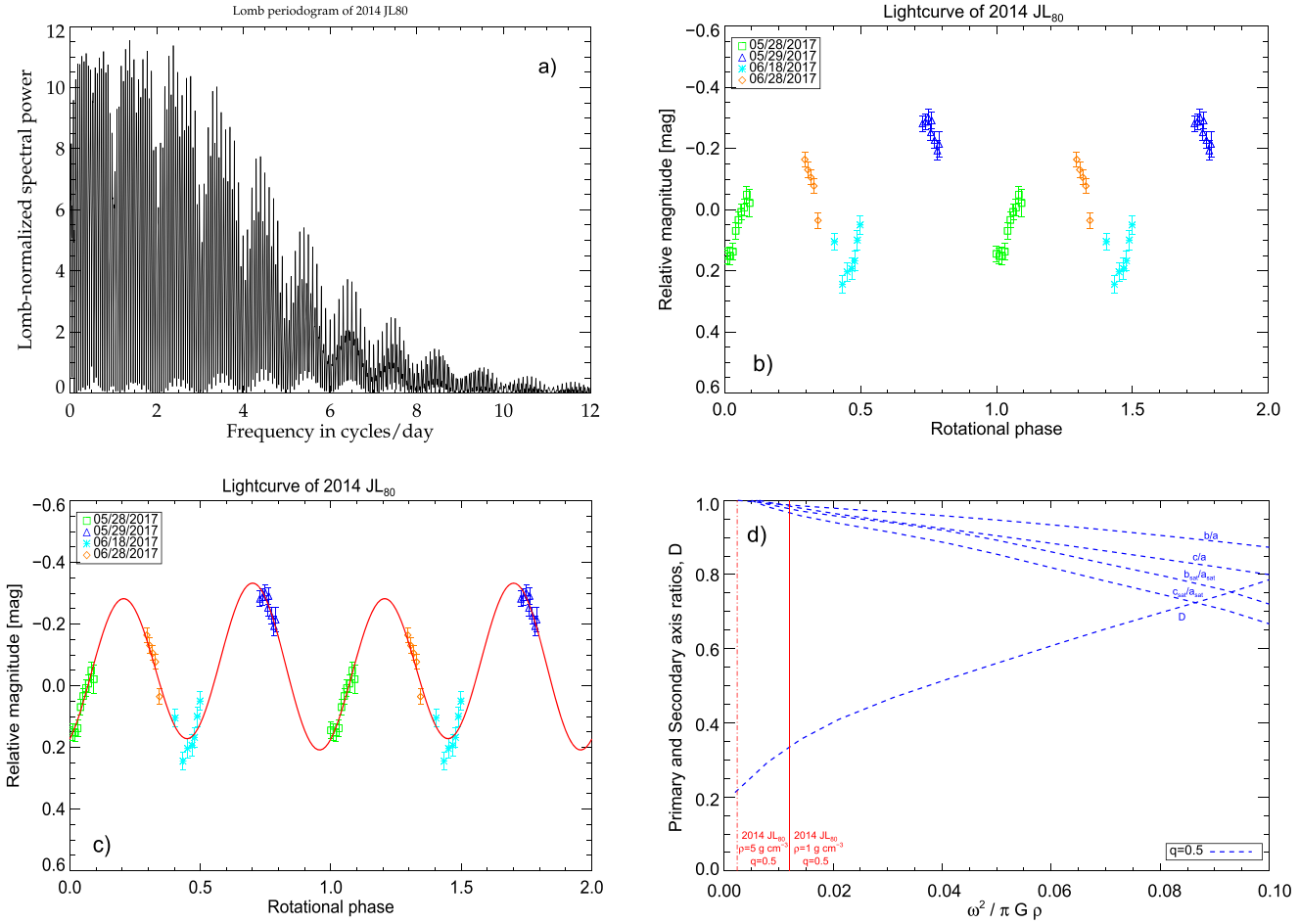

Figure 1. Study of 2014 JL_{80}: the Lomb periodogram presents several peaks, but the highest one suggests a double-peaked periodicity of 34.87 hr (plot (a)). The corresponding light curve is plotted on plot (b). We tried to fit a Fourier Series (second order) to our data (red continuous line, plot (c)), but the fit failed to reproduce the V-shape of the second minima. Because the light curve displays a large variability and because of the V-shape of the second peak, we suggest that this object is a contact binary. The plot (d) was used to derive the basic information of the system, assuming a contact binary nature.

Table 2
Summary of This Work

Object	P (hr)	Δm (mag)	φ_0 (JD) [2450000+]	H (mag)	Diameter (km)	Contact binary?
1995 HM_5	>0.6	>0.1	7893.81062	7.7	192/86	
(469362) 2001 KB_{77}	>4	>0.15	7922.69978	7.4	220/98	
2006 UZ_{184}	>2	>0.2	7356.78287	7.4	220/98	
2014 JK_{80}	>1	>0.17	7931.71324	6.1	400/179	
2014 JL_{80}	34.87	0.55 ± 0.03	7901.76240	7.1	253/113	Likely
2014 JO_{80}	6.32	0.60 ± 0.05	7922.51572	7.4	220/98	Likely
2014 JP_{80}	>0.5	>0.1	7931.85876	4.9	696/311	
2014 JQ_{80}	12.16	0.76 ± 0.04	7874.74484	7.0	265/118	Likely
2014 JT_{80}	>0.8	>0.1	7931.76831	7.1	253/113	
2014 KC_{102}	>4.5	>0.2	7922.70464	7.1	253/113	
2014 KX_{101}	>3	>0.2	7901.78398	7.4	220/98	
2015 BA_{519}	>4/8[a]	∼0.16	7874.73116	7.4	220/98	

Note. We report the preferred rotational period (P in hr), the full light-curve amplitude (Δm in mag), and the Julian Date (φ_0, no light-time correction) corresponding to the zero phase. Absolute magnitude (H), and the diameter considering an albedo of 0.04/0.2 are also indicated. In the case of a partial light curve, the lower limit to the period reported is the duration of our observing block.

[a] The light curve of 2015 BA_{519} shows a maximum and minimum over about 4 hr of observations. Therefore, the rotational period of this object is likely >8 hr (double-peaked).

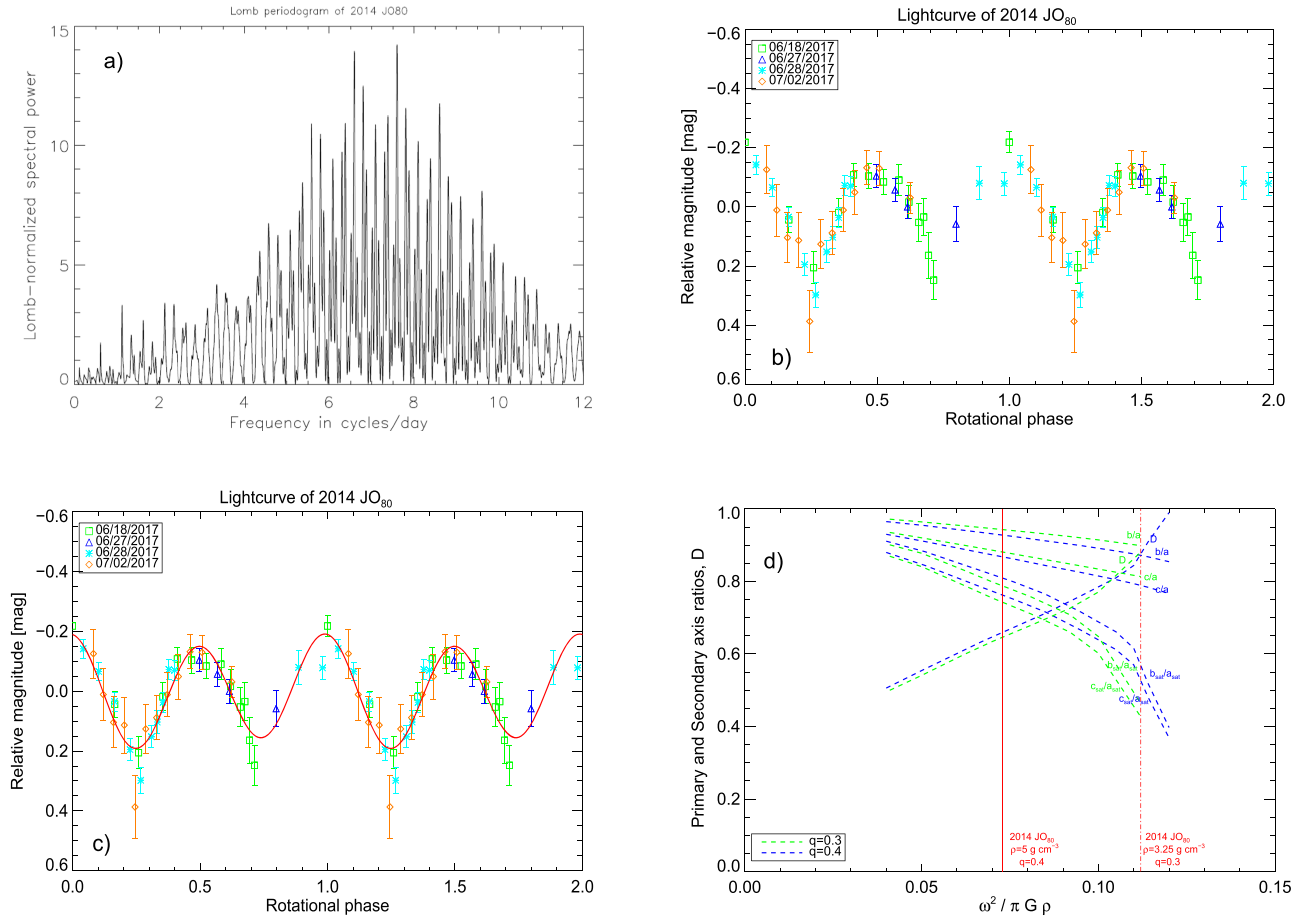

Figure 2. Study of 2014 JO_{80}: the highest peak of the Lomb periodogram favors a rotational period of 3.16 hr (plot (a)). However, based on the asymmetry of the light curve and the large amplitude, we favor the double-peaked option with a rotational period of 6.32 hr (plot (b)). A second-order Fourier Series fit is not able to reproduce the V- and U-shape of the light curve; therefore, we propose that 2014 JO_{80} is likely a contact binary (plot (c)). In order to derive basic information about the system, we used work from Leone et al. (1984) and summarized our results in plot (d).

2.1. Light Curves of Potential Contact Binaries

Now, the light curves of 2014 JL_{80}, 2014 JO_{80}, and 2014 JQ_{80} are displayed. All of these objects present a large variability between 0.55 and 0.76 mag and rotational periods from 6.32 hr up to almost 35 hr. These objects will be analyzed in detail in Section 3.

2.1.1. 2014 JL_{80}

With $H = 7.1$ mag as the absolute magnitude according to the Minor Planet Center (MPC), we estimate a size of 253/113 km (geometric albedo of 0.04/0.20).

After two nights of observations of 2014 JL_{80}, a very long rotational period of more than 24 hr and a large variability were suspected. Three more nights with sparse sampling observations were required to present a potential light curve. The highest peak of the Lomb periodogram corresponding to the single-peaked light curve is located at 1.38 cycles/day (17.44 hr, Figure 1). Assuming a double-peaked light curve, the rotational period is 34.87 hr. Such a slow rotation means that 2014 JL_{80} is one of the few slow rotators detected from ground-based observations with Pluto/Charon and 2010 WG_9 (Buie et al. 1997; Rabinowitz et al. 2013). In Figure 1, we plot the corresponding light curve with a variability of 0.55 mag. Unfortunately, we do not have the U-shape of the curve, but the V-shape of the second minima is visible. It is important to point out that the light curve of 2014 JL_{80} is very sparse, and thus the rotational period estimate needs to be improved. In Figure 1, one can appreciate that there are several aliases of the main peak located at 2.37 cycles/day (10.11 hr) and 0.77 cycles/day (31.03 hr). In all cases, the rotation of 2014 JL_{80} is very slow. For the purpose of the following work, we will use the main peak as the rotational period estimate.

A test using the FWHM of the light curve's peaks can suggest if an object is potentially a close binary or an elongated object (Thirouin & Sheppard 2017). In fact, by estimating the FWHM of the peaks, we have shown that the FWHM of the peaks are different in the case of a single and contact binary objects using their light curve plotted as magnitude versus rotational phase. Unfortunately, because the light curve of 2014 JL_{80} is sparse sampled, we are not able to provide an estimate for the U- and V-FWHM. But, based on the slow rotation of this object, we can argue that tidal effects due to a companion have affected the rotational period of this object (Thirouin et al. 2014). In fact, several TNOs (Pluto–Charon (Buie et al. 1997), Sila-Nunam (Grundy et al. 2012), and maybe 2010 WG_9 (Rabinowitz et al. 2013)) have rotational

periods longer than a day and are synchronously locked binaries.

Following the procedure described in Rabinowitz et al. (2013) and assuming that 2014 JL_{80} is an equal-sized binary system, we can estimate the separation between the two components. With a primary and a secondary having comparable diameters of 150 km, a density of 1000 kg m^{-3}, we calculate a ~320 km separation. Such a separation is below the resolution of the *HST* (Noll et al. 2008).

Because of the large variability and the second minima shape, 2014 JL_{80} is likely a contact binary or nearly a contact binary, and this case will be discussed in the following section.

2.1.2. 2014 JO_{80}

The absolute magnitude of 2014 JO_{80} is 7.4 mag (MPC value); thus, the diameter is 220/98 km using an albedo of 0.04/0.20.

With four nights of data, the Lomb periodogram favors a peak at 7.59 cycles/day (3.16 hr, Figure 2). There are also aliases of the main peak located at 6.58 cycles/day (3.65 hr) and 8.58 cycles/day (2.80 hr). All techniques used to confirm the periodicity favors the main peak, and thus we use this value for our work. Because of the large amplitude and because of an asymmetry of about 0.1 mag between the peaks, we favor the double-peaked light curve with a rotational period of 6.32 hr. The variability is 0.60 ± 0.05 mag (Figure 2).

Following Thirouin & Sheppard (2017), we estimate the U-FWHM at 0.38 and 0.37, and the V-FWHM at 0.16. Therefore, 2014 JO_{80} presents the same characteristic as the likely contact binaries reported in Thirouin & Sheppard (2017).

2.1.3. 2014 JQ_{80}

Based on the MPC estimate, the absolute magnitude of 2014 JQ_{80} is 7.0 mag, suggesting a diameter of 265/118 km with an albedo of 0.04/0.20.

With a total of 83 images obtained over two months in 2017, we report the first and unique light curve of 2014 JQ_{80}. The Lomb periodogram and the PDM technique favor a rotational period of 3.97 cycles/day (6.08 hr, Figure 3), but there are two aliases of this main peak with lower confidence levels at 2.95 cycles/day (8.13 hr) and 4.94 cycles/day (4.86 hr). In the following, we will use the main peak with the highest confidence level as the rotational periodicity. Because of the large amplitude of this object, we favor the double-peaked light curve with a rotational period of 12.16 hr. The light-curve amplitude is 0.76 ± 0.04 mag (Figure 3).

With the U-FWHM of 0.34 and 0.35 and the V-FHWM of 0.16 and 0.13, 2014 JQ_{80} meets the criteria mentioned in Thirouin & Sheppard (2017) for likely contact binaries.

Our study regarding the U-/V-FWHM is summarized in Figure 4. A complete description of this plot is available in Thirouin & Sheppard (2017).

2.2. Partial Light Curves

2.2.1. 1995 HM_5

1995 HM_5 is the smallest object in our sample. With an absolute magnitude of 7.7 mag, its diameter is between 86 and 192 km assuming geometric albedos of 0.04 and 0.2, respectively. We report about 0.6 hr of observations obtained in 2017 May. Our few observations show a minimum variability of ~0.1 mag (Figure 5). Based on our data, no rotational period is derived.

2.2.2. (469362) 2001 KB_{77}

We report six images of 2001 KB_{77} obtained on UT 18 June. In about 4 hr, 2001 KB_{77} displays a variability of 0.15 mag (Figure 5). To our knowledge, there is no bibliographic reference to compare our result with. No rotational period is derived from our observations, so we can only constrain the period to be longer than 4 hr.

2.2.3. 2006 UZ_{84}

We observed 2006 UZ_{184} over two consecutive nights in 2015 November–December. Unfortunately, due to bad weather conditions, only 10 images were usable. Over two nights, this object seems to have a variability of about 0.2 mag, and no period is derived (Figure 5).

2.2.4. 2014 JK_{80}

2014 JK_{80} was studied over two consecutive nights at the end of 2017 June. Data from the first night do not show an obvious sign of variability, but the second night shows a variability of about 0.17 mag (Figure 5).

2.2.5. 2014 JP_{80}

2014 JP_{80}, with $H = 4.9$ mag, a diameter of 698/311 km considering an albedo of 0.04/0.2 is the largest object here. With only five images obtained over about 0.5 hr, it is difficult to provide any reliable conclusion regarding 2014 JP_{80}. The partial light curve shows a variability of ~0.1 mag (Figure 5).

2.2.6. 2014 JT_{80}

We have five images of 2014 JT_{80} obtained over about 1 hr in June 27, but only three images were usable. The variabilty is about 0.1 mag (Figure 5).

2.2.7. 2014 KC_{102}

We have two nights of data for 2014 KC_{102}. The second night shows the maximum of the curve with a variability of around 0.2 mag over 4.5 hr of observations (Figure 5). Therefore, considering a double-peaked light curve, we suggest a rotational period of about 9 hr, but more data are needed for a better estimate.

2.2.8. 2014 KX_{101}

We report two consecutive nights of observations for 2014 KX_{101}. Both nights are showing a variability of about 0.2 mag (Figure 5). Unfortunately, no rotational period estimate is derived.

2.2.9. 2015 BA_{519}

2015 BA_{519} was observed during only one night on UT May 1. In a couple of hours of observations, a variability of ~0.16 mag is noticed. The partial light curve plotted in Figure 5 presents one maximum and one

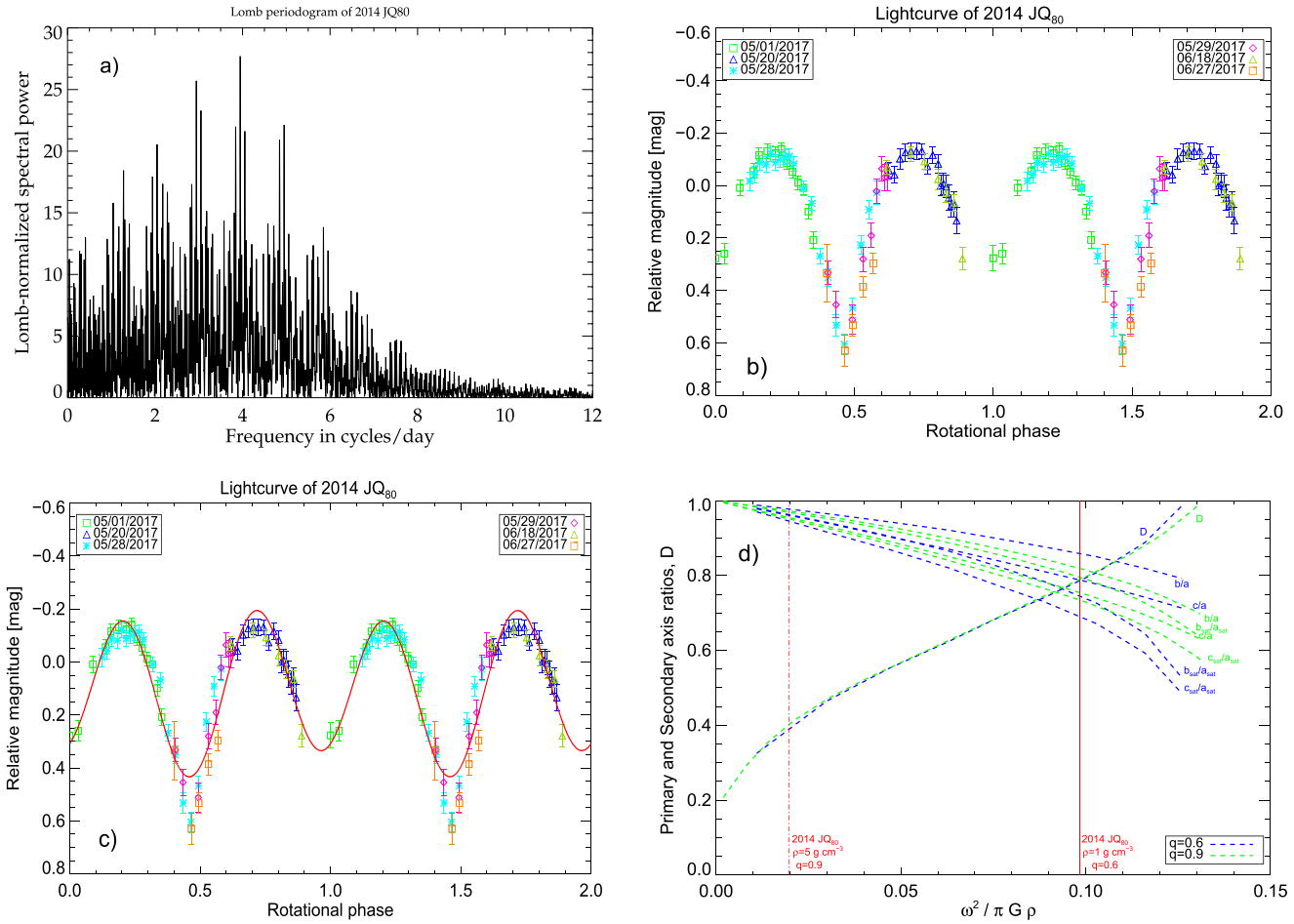

Figure 3. Study of 2014 JQ_{80}: based on the Lomb periodogram study, we estimate that 2014 JQ_{80} has a double-peaked light curve with a rotational period of 12.16 hr (plot (a)). Because the light curve displays a large variability, and because of the V-/U-shapes of the minima/maxima, we suggest that this object is a contact binary (plot b), and (c). The plot (d) was used to derive the basic information of the system, assuming a contact binary nature.

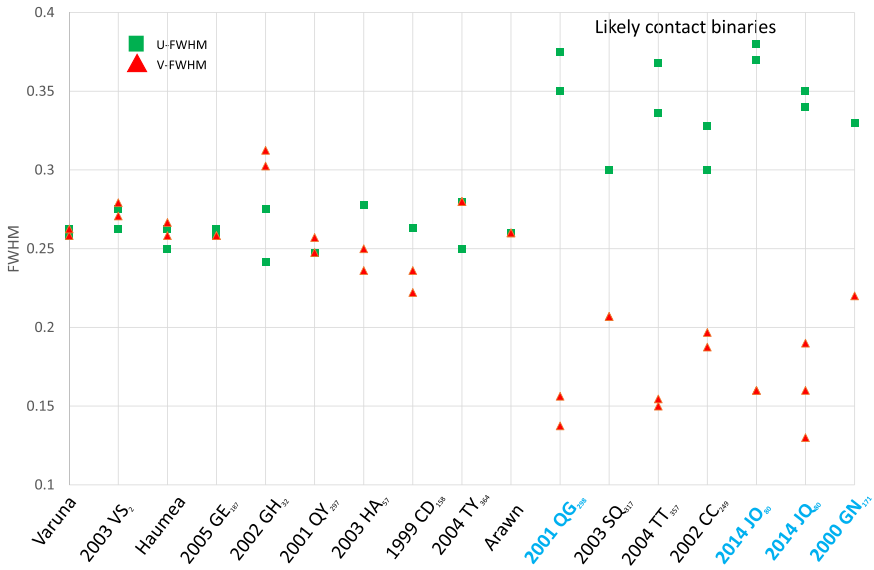

Figure 4. FWHM of single objects, resolved binaries and (likely/confirmed) contact binaries: a complete description of this plot is available in Thirouin & Sheppard (2017). The (likely/confirmed) contact binaries present a U-FWHM $\geqslant 0.30$ and a V-FWHM $\leqslant 0.22$. Likely contact binaries in the Plutino population have their names highlighted in light blue. This study made use of light curves plotted as magnitude vs. rotational phase.

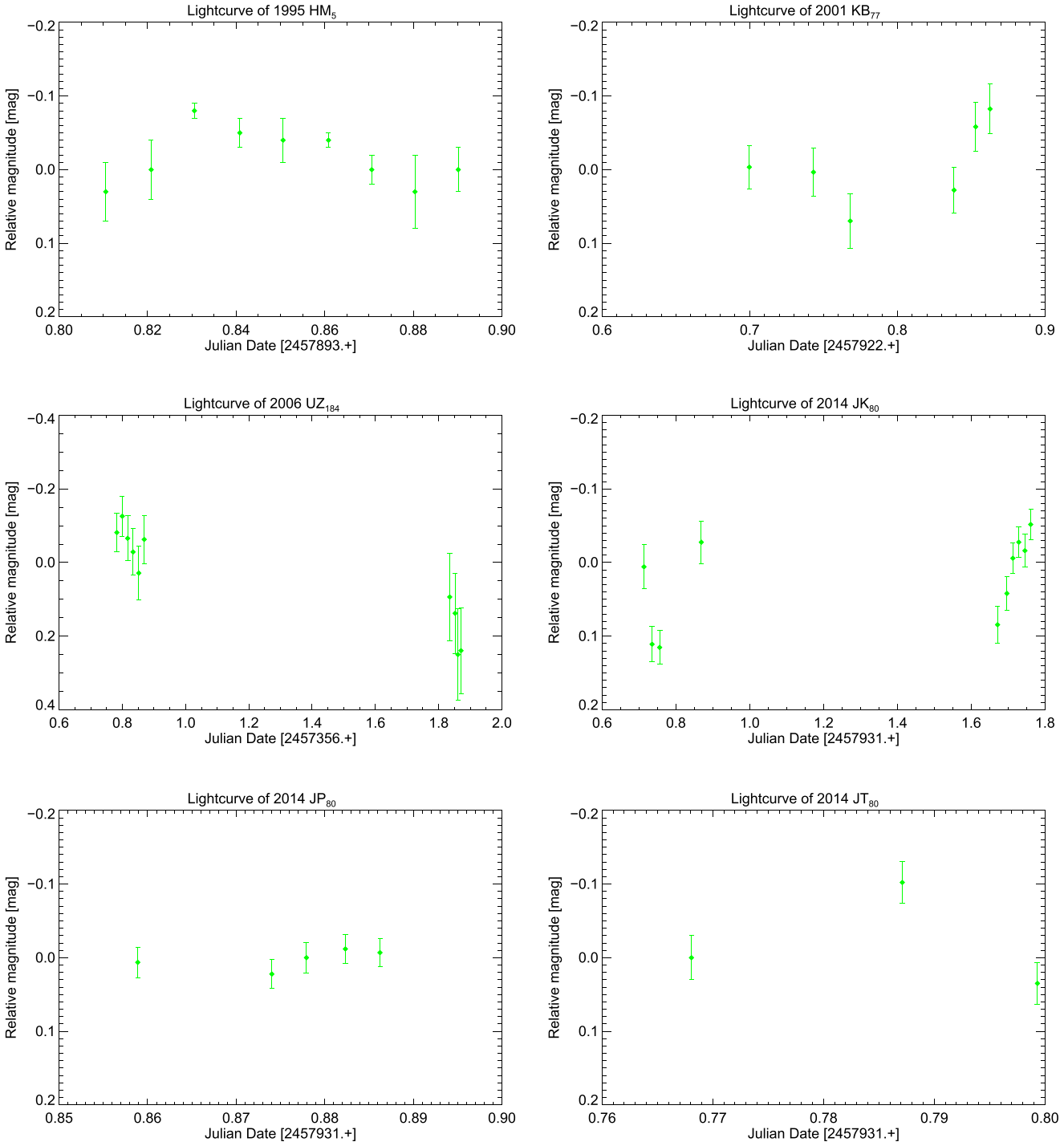

Figure 5. Partial light curves of several Plutinos: we report relative magnitude vs. Julian Date (no light-time correction) for nine objects.

minimum, so the rotational period of this object should be approximately 8 hr (assuming a double-peaked light curve). No additional information about this object has been found in the literature.

3. Analysis

Next, we consider a contact binary configuration and a single very elongated object option to explain the high light-curve variability of 2014 JL_{80}, 2014 JO_{80}, and 2014 JQ_{80}.

3.1. Roche System

The large light-curve amplitudes of 2014 JL_{80}, 2014 JO_{80}, and 2014 JQ_{80} are best explained if these objects are classified as contact binary systems. In the following section, we constrain basic information about the systems Leone et al. (1984). We estimate the mass ratio and the density using the Roche sequences (Figure 6). Following Leone et al. (1984) assumptions, we derive min and max cases. The density range in Leone et al. (1984) is limited to $\rho = 1000$–$5000\,\mathrm{kg\,m^{-3}}$, but lower densities are possible for the TNOs.

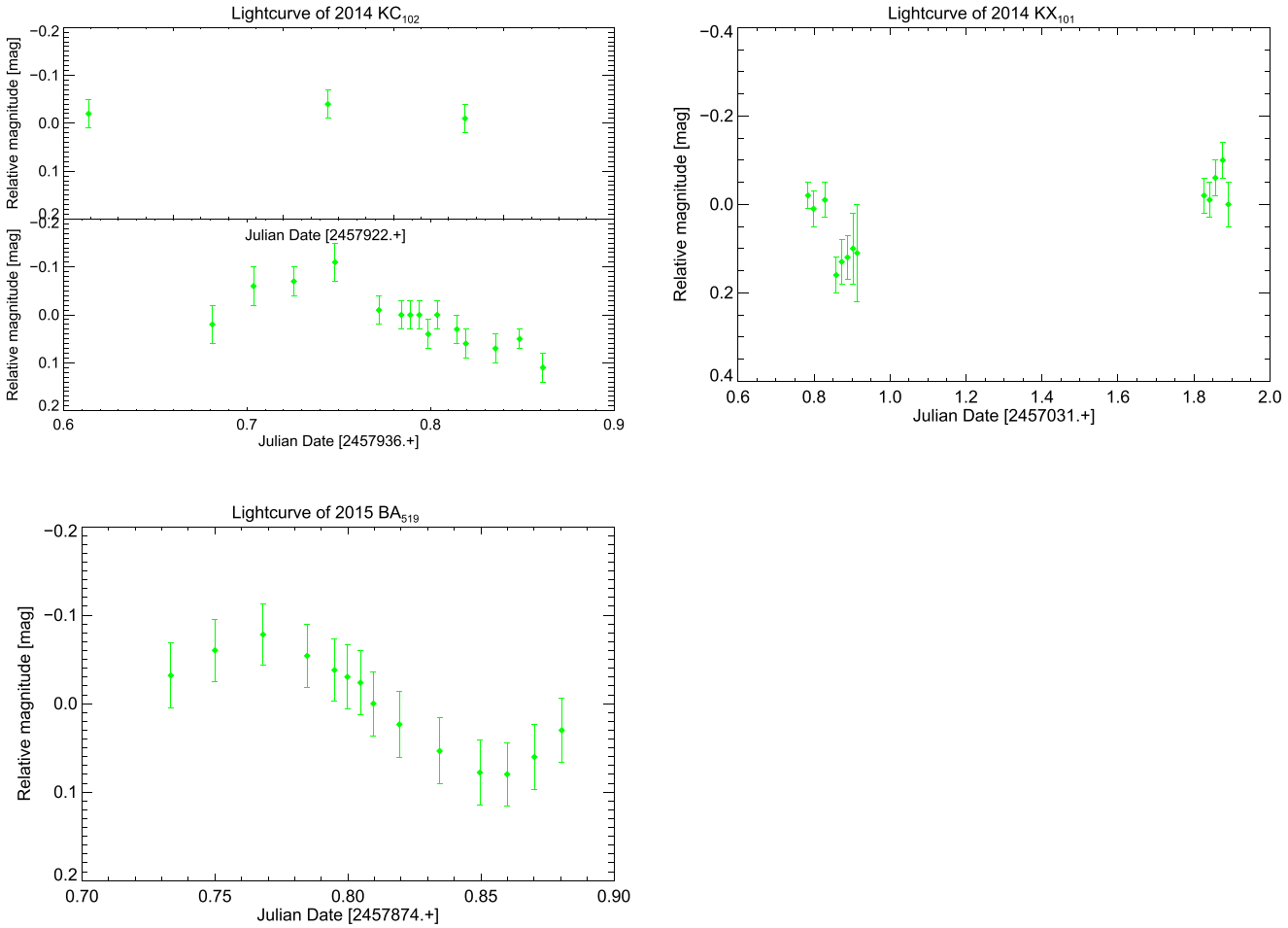

Figure 5. (Continued.)

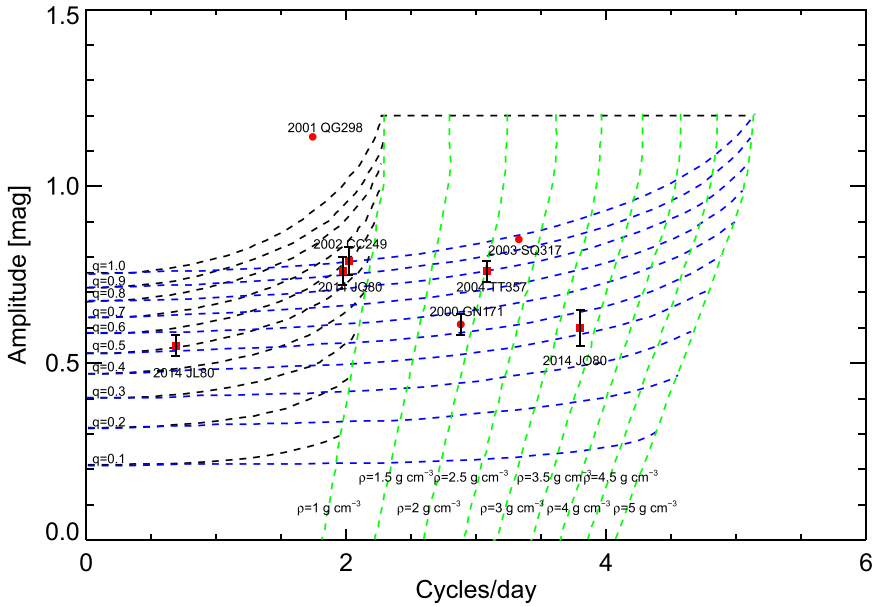

Figure 6. The network of Roche sequences: a complete description of this plot is available in Leone et al. (1984) and Thirouin et al. (2017). Confirmed/likely contact binaries from this work and the literature are plotted. The names of each object are also indicated.

3.1.1. 2014 JL_{80}

For 2014 JL_{80}, based on Leone et al. (1984), we estimate that $q_{min} \sim q_{max} \sim 0.5$, whereas the density range is $\rho_{min} = 1000\,kg\,m^{-3}$, $\rho_{max} = 5000\,kg\,m^{-3}$.

Considering 2014 JL_{80} as a binary with a mass ratio of 0.5 and a density of $1000\,kg\,m^{-3}$, the axis ratios of the primary are: $b/a = 0.99$, $c/a = 0.98$ ($a = 71/31$ km, $b = 71/31$ km, and $c = 70/31$ km assuming an albedo of 0.04/0.2), the axis ratios of the secondary are: $b_{sat}/a_{sat} = 0.98$, $c_{sat}/a_{sat} = 0.97$ ($a_{sat} = 57/26$ km, $b_{sat} = 56/26$ km, and $c_{sat} = 55/25$ km with an albedo of 0.04/0.2). The parameter D is 0.34; thus, the distance between bodies is 378/169 km (albedo of 0.04/0.2).

3.1.2. 2014 JO_{80}

For 2014 JO_{80}, we have: (i) a system with $q_{min} = 0.3$ and $\rho_{min} = 3.25\,g\,cm^{-3}$ or (ii) a system $q_{max} = 0.42$ and $\rho_{max} = 5\,g\,cm^{-3}$. Based on the light-curve amplitude, the uncertainty for the mass ratio is $\pm$ 0.07. If 2014 JO_{80} is a binary system with a mass ratio of 0.3 and a density of $3.25\,g\,cm^{-3}$, we derive the axis ratios of the primary: $b/a = 0.90$, $c/a = 0.81$ ($a = 75/33$ km, $b = 68/30$ km, and $c = 61/27$ km assuming an albedo of 0.04/0.2), and the axis ratios of the secondary: $b_{sat}/a_{sat} = 0.46$, $c_{sat}/a_{sat} = 0.43$ ($a_{sat} = 79/36$ km, $b_{sat} = 36/16$ km, and $c_{sat} = 34/15$ km assuming an albedo of 0.04/0.2). The separation between the components is 175/78 km with an albedo of 0.04/0.2, assuming $D = 0.88$.

3.1.3. 2014 JQ_{80}

For 2014 JQ_{80}, we compute two extreme options: (i) a system with $q_{min} = 0.57$ and $\rho_{min} = 1\,g\,cm^{-3}$ or (ii) a system with $q_{max} = 0.92$ and $\rho_{max} = 5\,g\,cm^{-3}$. Here, we will consider a conservative mass ratio of $q_{min} = 0.6$.

If 2014 JQ_{80} is a binary with $q = 0.6$, and $\rho = 1\,g\,cm^{-3}$, we obtain for the primary: $b/a = 0.86$, $c/a = 0.79$ ($a = 84/37$ km, $b = 72/32$ km, and $c = 66/29$ km assuming an albedo of 0.04/0.2), for the secondary: $b_{sat}/a_{sat} = 0.75$, $c_{sat}/a_{sat} = 0.69$ ($a_{sat} = 78/35$ km, $b_{sat} = 59/26$ km, and $c_{sat} = 54/24$ km assuming an albedo of 0.04/0.2). The separation between the components is 208/92 km with an albedo of 0.04/0.2 and $D = 0.78$.

The typical density in the Kuiper Belt is $\sim$1 $g\,cm^{-3}$, with the exceptions of a few denser bigger objects (Sheppard et al. 2008; Grundy et al. 2012; Brown 2013; Vilenius et al. 2014; Thirouin et al. 2016). Therefore, we have not previously derived axis ratios and separation assuming a high density $\rho_{max} = 5\,g\,cm^{-3}$. It is important to point out that careful modeling of these systems using several light curves obtained for different epochs will be necessary to derive accurate basic parameters for all of them.

3.2. Jacobi Ellipsoid

The light curves of 2014 JL_{80}, 2014 JO_{80}, and 2014 JQ_{80} are not reproduced by a second-order Fourier series fit because of their U-/V-shapes. Therefore, we favor the option of contact binary to explain these light curves, but if these objects are single Jacobi ellipsoids, we can constrain their elongations and densities (Thirouin et al. 2017; Thirouin & Sheppard 2017).

3.2.1. 2014 JL_{80}

In the case of 2014 JL_{80}, considering a viewing angle of 90°, we find $a/b = 1.67$, and $c/a = 0.44$ (Chandrasekhar 1987). So, we compute: $a = 213$ km ($a = 95$ km), $b = 128$ km ($b = 57$ km), and $c = 94$ km ($c = 42$ km) for an albedo of 0.04 (0.20) and an equatorial view. Using a viewing angle of 60°, we derive an axis ratio $a/b > 2.31$. As ellipsoids with $a/b > 2.31$ are unstable to rotational fission, the viewing angle of 2014 JL_{80} must be larger than 62°.5 (Jeans 1919). With an equatorial view, the density is $\rho \geqslant 0.04\,g\,cm^{-3}$. The very long rotation of 2014 JL_{80} likely means that this object cannot be a Jacobi ellipsoid, which generally are fast rotators and have high angular momentum (Sheppard et al. 2008).

3.2.2. 2014 JO_{80}

Assuming an equatorial view, we compute $a/b = 1.72$, and $c/a = 0.42$. Therefore, the axes are: $a = 170$ km ($a = 85$ km), $b = 99$ km ($b = 49$ km), and $c = 71$ km ($c = 36$ km) for an albedo of 0.04 (0.20) and an equatorial view. As for 2014 JL_{80}, a viewing angle of 60° suggests that 2014 JO_{80} is unstable to rotational fission. We estimate that the aspect angle is between 65° and 90°. Using an equatorial view, the density is $\rho \geqslant 1100\,kg\,m^{-3}$. The very short period of 2014 JO_{80} makes a Jacobi-type object likely because of its high angular momentum.

3.2.3. 2014 JQ_{80}

With an equatorial view for 2014 JQ_{80}, we obtain $a/b = 2$, and $c/a = 0.38$. Therefore, we compute: $a = 248$ km ($a = 111$ km), $b = 124$ km ($b = 55$ km), and $c = 94$ km ($c = 42$ km) for an albedo of 0.04 (0.20) and an equatorial view. 2014 JQ_{80} is stable to rotational fission if its viewing angle is larger than 74°. Assuming $\xi = 90°$, the density is $\rho \geqslant 0.32\,g\,cm^{-3}$.

In conclusion, to explain the morphology of the light curves of 2014 JL_{80}, 2014 JO_{80}, and 2014 JQ_{80}, we showed details of a single elongated object or close binary configuration. However, because of the V-/U-shape and the extreme variability, we favor the contact binary explanation. Future observations are required to infer the nature of 2014 JL_{80}, 2014 JO_{80}, and 2014 JQ_{80}. In all cases, we selected the rotational periods favored by the main peaks (i.e., peak with the highest confidence level) because the options from the aliases produced the worst quality light curves.

4. Percentage of Contact Binaries

4.1. Status of the Plutino Light Curve Studies

Tables 2 and 3 summarize the short-term variability studies of Plutinos published in this work and in the literature (respectively). In total, 39 Plutinos[3] have been observed for light curves: 12 Plutinos are reported in this paper and 27 in the literature. However, only 21 objects have a rotational period (secure result and tentative); the rest have only light-curve amplitude constraints.

Based on Table 3, one can appreciate that most of the Plutinos display a low light-curve amplitude with a mean value of $\sim$0.13 mag (Figure 7). But, several objects are showing larger

[3] To date, 225 Plutinos are known. So, based on published results, only $\sim$17% of the Plutinos have been observed for light curves.

Table 3
Summary of Short-term Variability of the Plutino Trans-Neptunian Objects

Object	Single-peaked period (hr)	Double-peaked period (hr)	Δm (mag)	H (mag)	References
(134340) Pluto	153.2	⋯	0.33	−0.7	B97
Charon	153.6	⋯	0.08	0.9	B97
(15789) 1993 SC	7.7129	⋯	0.5	7.0	W95
	⋯	⋯	<0.2	⋯	T97, D97[a]
(15810) 1994 JR_1 Arawn	⋯	5.47 ± 0.33	0.58	7.7	P16
(15820) 1994 TB	3.0/3.5	6.0/7.0	0.26/0.34	7.3	RT99
	⋯	⋯	<0.04	⋯	SJ02
(32929) 1995 QY_9	⋯	7.3 ± 0.1	0.60 ± 0.04	8.0	RT99, SJ02
(15875) 1996 TP_{66}	1.96	⋯	<0.04	7.0	CB99[b]
	⋯	⋯	<0.12	⋯	RT99
(118228) 1996 TQ_{66}	⋯	⋯	<0.22	6.9	RT99
(91133) 1998 HK_{151}	⋯	⋯	<0.15	7.6	SJ02
(33340) 1998 VG_{44}	⋯	⋯	<0.10	6.5	SJ02
(47171) 1999 TC_{36}	6.21 ± 0.02	⋯	0.06	4.9	O03
	⋯	⋯	<0.07	⋯	LL06
	⋯	⋯	<0.05	⋯	SJ03
(38628) 2000 EB_{173} Huya	(6.68/**6.75**/6.82) ± 0.01	⋯	<0.1	4.8	O03
	⋯	⋯	<0.15	⋯	SJ02
	⋯	⋯	<0.06	⋯	SR02
	⋯	⋯	<0.04	⋯	SJ03, LL06
	5.21	⋯	0.02 ± 0.01	⋯	T14
	4.45 ± 0.07	⋯	∼0.1	⋯	G16
2000 FV_{53}	⋯	7.5	0.07 ± 0.02	8.3	TB06
(47932) 2000 GN_{171}	⋯	8.329 ± 0.005	0.61 ± 0.03	6.2	SJ02
	⋯	⋯	0.53	⋯	D08[c]
	⋯	⋯	0.64 ± 0.11	⋯	R07
2001 KD_{77}	⋯	⋯	<0.07	5.8	SJ03
(469372) 2001 QF_{298}	⋯	⋯	<0.12	5.2	SJ03
	⋯	⋯	∼0.11	⋯	T13
(139775) 2001 QG_{298}	6.8872 ± 0.0002	13.7744 ± 0.0004	1.14 ± 0.04	6.9	SJ04
	⋯	13.7744 ± 0.0004	0.7 ± 0.01	⋯	L11
(28978) 2001 KX_{76} Ixion	⋯	⋯	<0.05	3.6	O03, SJ03
	15.9 ± 0.5	⋯	0.06 ± 0.03	⋯	RP10
	12.4 ± 0.3	⋯	⋯	⋯	G16
(55638) 2002 VE_{95}	(6.76/6.88/7.36/9.47) ± 0.01	⋯	0.08 ± 0.04	5.5	O06
	⋯	⋯	<0.06	⋯	SJ03
	9.97	⋯	0.05 ± 0.01	⋯	T10
(208996) 2003 AZ_{84}	(4.32/5.28/6.72/**6.76**) ± 0.01	⋯	0.10 ± 0.04	3.7	O06
	6.72 ± 0.05	⋯	0.14 ± 0.03	⋯	SJ03
	6.79	⋯	0.07 ± 0.01	⋯	T10
	6.78	⋯	0.07 ± 0.01	⋯	T14
2003 HA_{57}	⋯	6.44	0.31 ± 0.03	8.1	T16
(455502) 2003 UZ_{413}	⋯	4.13 ± 0.05	0.13 ± 0.03	4.3	P09
(84922) 2003 VS_2	(3.71 or 4.39) ± 0.01	⋯	0.23 ± 0.07	4.2	O06
	⋯	7.41 ± 0.02	0.21 ± 0.02	⋯	S07
	⋯	7.42	0.21 ± 0.01	⋯	T10
	⋯	7.4208	0.224 ± 0.013	⋯	T13
(90482) 2004 DW Orcus	7.09/**10.08 ± 0.01**/17.43	**20.16**	0.04 ± 0.02	2.2	O06
	13.19	⋯	0.18 ± 0.08	⋯	R07
	⋯	⋯	<0.03	⋯	S07
	10.47	⋯	0.04 ± 0.01	⋯	T10
	11.9 ± 0.5	⋯	⋯	⋯	G16
(469708) 2005 GE_{187}	6.1	⋯	0.5	7.3	S10
	⋯	11.99	0.29 ± 0.02	⋯	T16
(469987) 2006 HJ_{123}	⋯	⋯	<0.13	5.9	BS13
(341520) 2007 TY_{430} Mors–Somnus	⋯	9.28	0.24 ± 0.05	6.9	T14[d]

Notes. Preferred rotational period is indicated in bold. Reference list is after the table.
[a] Results from Williams et al. (1995) were not supported by Tegler et al. (1997), and Davies et al. (1997). Thus, this object will not be considered in our study.
[b] Rotational period of 1996 TP_{66} is likely wrong and will not be used in this work.
[c] Dotto et al. (2008) used the rotational period from Sheppard & Jewitt (2002) to fit their data. They reported a light-curve amplitude of 0.60 ± 0.03 mag, but based on their fit (Figure 3 of Dotto et al. 2008), the light-curve amplitude is about 0.53 mag.
[d] According to Sheppard et al. (2012), 2007 TY_{430} is a dynamically cold classical object in the Plutino population.
References. W95: Williams et al. (1995), B97: Buie et al. (1997), D97: Davies et al. (1997), T97: Tegler et al. (1997), CB99: Collander-Brown et al. (1999), RT99: Romanishin & Tegler (1999), SJ02: Sheppard & Jewitt (2002), SR02: Schaefer & Rabinowitz (2002), O03: Ortiz et al. (2003), SJ03: Sheppard & Jewitt (2003), SJ04: Sheppard & Jewitt (2004), LL06: Lacerda & Luu (2006), O06: Ortiz et al. (2006), TB06: Trilling & Bernstein (2006), R07: Rabinowitz et al. (2007), S07: Sheppard (2007), D08: Dotto et al. (2008), P09: Perna et al. (2009), RP10: Rousselot & Petit (2010), S10: Snodgrass et al. (2010), T10: Thirouin et al. (2010), L11: Lacerda (2011), BS13: Benecchi & Sheppard (2013), T13: Thirouin (2013), T14: Thirouin et al. (2014), G16: Galiazzo et al. (2016), P16: Porter et al. (2016), T16: Thirouin et al. (2016).

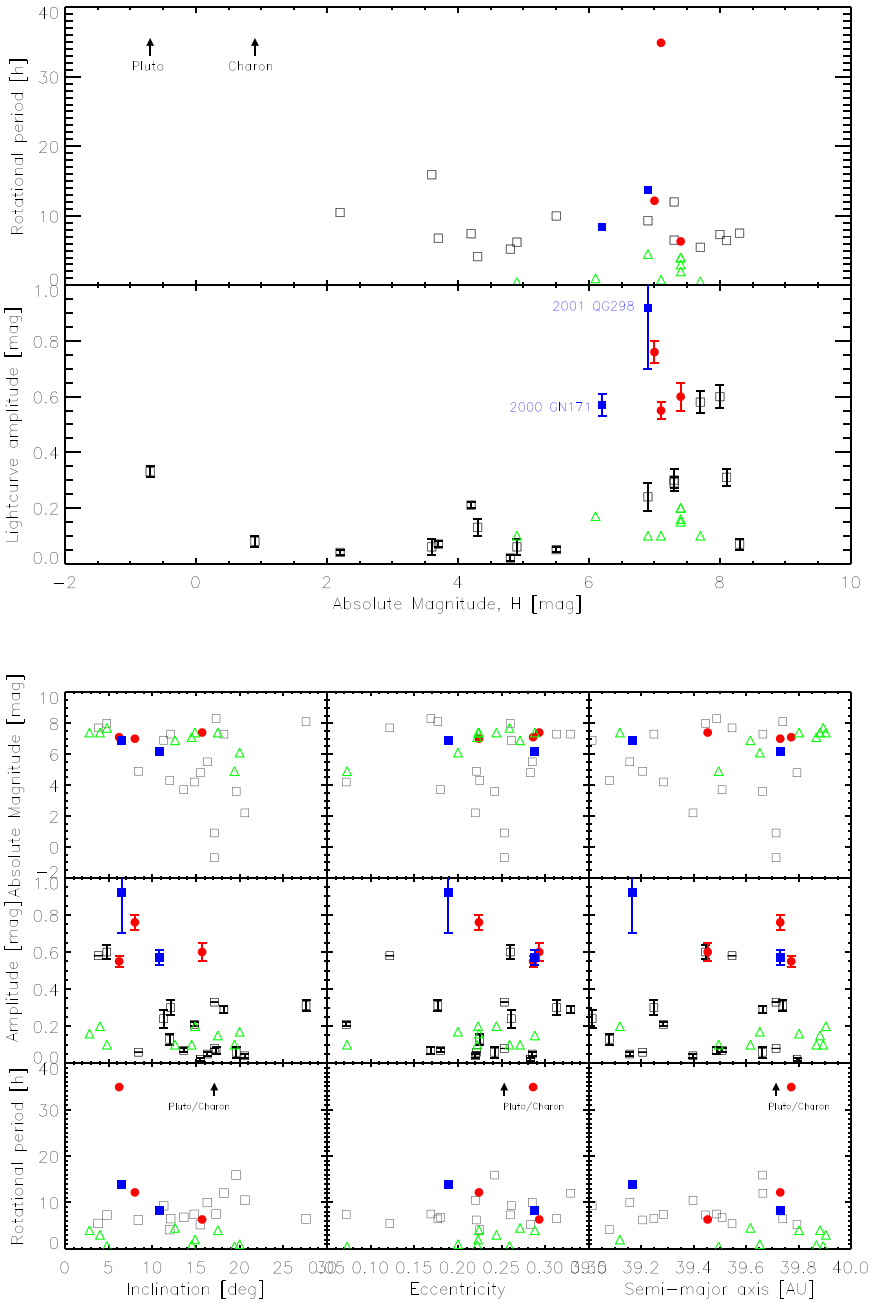

Figure 7. Rotational properties and orbital elements: all of the Plutinos with published light curves are plotted. Open black squares are from the literature; green triangles are plutinos with partial light curves reported in this work (lower estimates for the period and amplitude); red circles are the likely contact binaries from this wor; blue circles are the likely/confirmed contact binaries from the literature. There is a correlation between amplitude and absolute magnitude and an anti-correlation between inclination and light-curve amplitude.

variability: Pluto, Arawn (1994 JR_1), 1995 QY_9, 2000 GN_{171}, and 2001 QG_{298}. The NASA's New Horizons flyby of Pluto confirmed that the light-curve amplitude is due to a strong albedo contrast on Pluto's surface, whereas 2001 QG_{298} is a contact binary (Sheppard & Jewitt 2004; Buratti et al. 2017). Arawn, also observed by New Horizons at a very high phase angle, displays an amplitude of 0.58 mag[4] based on the fit reported in Porter et al. (2016). We estimate the V-FWHM and the U-FWNM of Arawn and find that the U-FWHM and the V-FWHM are about the same (∼0.26). Therefore, following the criteria reported in Thirouin & Sheppard (2017), Arawn is likely not a contact binary, and thus its large amplitude is due to an elongated shape. However, the Arawn observations were performed at a phase angle up to ∼59° whereas the typical ground-based TNO light curves are obtained at a phase angle up to ∼2°. With such a high phase angle compared to Earth observations, it is difficult to directly compare the light-curve morphologies, as the shadowing effect is not negligible. Therefore, the direct comparison of ground- and space-based light curves can be wrong. In the case of 1995 QY_9, only one light curve is reported in the literature (Romanishin & Tegler 1999). The light-curve amplitude is about 0.6 mag. Unfortunately, no further study of this object can confirm or disprove such a finding, and we cannot use the V-/U-FWHM

[4] Porter et al. (2016) reported an amplitude of 0.8 mag as the difference between the highest and lowest point of the curve.

technique, as the photometry is not available and the light curve plotted is not phased folded.

The light curve of 2000 GN_{171} displays a large variability of ~0.6 mag (Sheppard & Jewitt 2002; Rabinowitz et al. 2007). It has been suggested that the light curve of 2000 GN_{171} is due to an elongated shape, but the option of a contact binary system was not excluded (Sheppard & Jewitt 2002). Later, based on light-curve modeling Lacerda & Jewitt (2007) suggested that the Roche and Jacobi solution are equivalent and thus could not favor any option regarding the nature of this object/system. Using the Sheppard & Jewitt (2002) light curve, we estimate an U-FWHM of 0.33 and a V-FHWM of 0.22 and 0.19; therefore, according to our study reported in Thirouin & Sheppard (2017), 2000 GN_{171} is likely a contact binary (Figure 4). The most recent light curve of 2000 GN_{171} was obtained in 2007 by Dotto et al. (2008). They obtained a rotational period consistent with Sheppard & Jewitt (2002) result, and they argue that the light-curve amplitude is also similar. However, based on their Figure 3, the light-curve amplitude is smaller than reported. Their photometry is not available online, but using their plot, the amplitude seems to be around 0.53 mag. In conclusion, there is a potential change in the light-curve amplitude and thus potentially a change in the system orientation between the first and last light curve obtained in 2001 and 2007. A careful modeling of those light curves may infer the nature of the system/object.

In conclusion, 2000 GN_{171} is likely a contact binary, and a change in the light-curve amplitude is potentially observable. In the case of 1995 QY_9, a new light curve will be useful to constrain the nature of this object. For the purpose of our study, we will assume that this object is a single elongated one, as it is the case for Arawn.

4.2. Fraction of Contact Binaries in the Plutino Population

With the literature and this work, we have evidence that five likely/confirmed contact binaries are in the Plutino population, not including the large-amplitude objects 1995 QY_9 and Arawn, as we assume they are elongated but not contact binaries. We'd like to point out that these five likely/confirmed contact binaries are based on the literature data and the objects observed for this work (i.e., 5 out of 39 objects). Such a number seems to indicate that the Plutino population may have a large reservoir of contact binaries compared to the other populations (Sheppard & Jewitt 2004; Lacerda et al. 2014; Thirouin et al. 2017; Thirouin & Sheppard 2017). It is important to point out that a threshold of 0.9 mag has been used in the literature to identify a contact binary, but a non-equal-sized close system may never pass such a threshold even if observed equator-on. Therefore, in the following paragraphs, we will use several light-curve amplitude limits. We also assume that the partial light curves reported in this work are due to noncontact binary objects. However, some of these may be contact binaries with very long rotational periods, and thus their identification is not possible based on our data. Therefore, the fractions of contact binaries reported below are lower limits.

Following the procedure detailed in Sheppard & Jewitt (2004), we calculate the percentage of close binaries in the Plutino population.

In the first approximation, we assume that the light-curve amplitude of an object with axes $a > b$, and $b = c$ varies following:

$$\Delta_m = 2.5 \log\left(\frac{1+\tan\theta}{(b/a)+\tan\theta}\right). \quad (1)$$

θ is the angle of the object's pole relative to the perpendicular of the sight line. An amplitude of 0.9 mag is reached at $\theta = 10°$ for an object with an elongation of $a/b = 3$. Therefore, the probability of observing an object from a random distribution within 10° of the sight line is $P(\theta \leqslant 10°) = 0.17$. With the same approach, we estimate that an amplitude of 0.5 mag is reached at $\theta = 36°$, whereas an amplitude of 0.6 mag is reached at $\theta = 27°$, and an amplitude of 0.7 mag is reached at $\theta = 20°$. In our sample of 12 objects, we have one TNO with a $\Delta_m \geqslant 0.7$ mag. Thus, the detection of one TNO with $\Delta_m \geqslant 0.7$ mag implies that the abundance of similar objects is: $f(\Delta_m \geqslant 0.7\,\mathrm{mag}) \sim 1/(12{*}P(\theta \leqslant 20°)) \sim 25\%$. Similarly, we estimate: $f(\Delta_m \geqslant 0.6\,\mathrm{mag}) \sim 2/(12{*}P(\theta \leqslant 27°)) \sim 37\%$, and $f(\Delta_m \geqslant 0.5\,\mathrm{mag}) \sim 3/(12{*}P(\theta \leqslant 36°)) \sim 42\%$. Using our sample and the literature, we calculate: $f(\Delta_m \geqslant 0.7\,\mathrm{mag}) \sim 28\%$, $f(\Delta_m \geqslant 0.6\,\mathrm{mag}) \sim 42\%$, and $f(\Delta_m \geqslant 0.5\,\mathrm{mag}) \sim 40\%$. Theses estimates do not include 1995 QY_9 and Arawn as we assume they are elongated objects.

In a second approximation, and assuming a triaxial Jacobi with $a \geqslant b = c$, the light-curve variability is (Sheppard & Jewitt 2004):

$$\Delta_m = 2.5 \log\left(\frac{a}{b}\right) - 1.25 \log\left(\left(\left(\frac{a}{b}\right)^2 - 1\right)\sin^2\theta + 1\right). \quad (2)$$

With the same approach as previously used, we find for our sample: $f(\Delta_m \geqslant 0.7\,\mathrm{mag}) \sim 19\%$, $f(\Delta_m \geqslant 0.6\,\mathrm{mag}) \sim 34\%$, $f(\Delta_m \geqslant 0.5\,\mathrm{mag}) \sim 44\%$. Using both the literature and our sample, we compute: $f(\Delta_m \geqslant 0.7\,\mathrm{mag}) \sim 22\%$, $f(\Delta_m \geqslant 0.6\,\mathrm{mag}) \sim 39\%$, $f(\Delta_m \geqslant 0.5\,\mathrm{mag}) \sim 42\%$. It is important to mention that we are considering that the sparse light curves with low to moderate amplitudes reported here are due to single objects. In some cases, our temporal coverage is limited and some objects may be contact binaries with very slow rotation, like 2014 JL_{80}. Therefore, our estimates are lower limits.

Ten objects in our sample have absolute magnitude $H \geqslant 7.0$ mag (diameter of 265/118 mag with albedo of 0.04/0.2). So far, observers have been focusing on large and bright TNOs, with only a handful of studies of smaller objects (see Thirouin (2013) for a complete review). Therefore, we are testing a new size range of objects, and only little information is known about rotational properties of medium to small TNOs. In Figure 7, one can appreciate that the light-curve amplitude is increasing at higher absolute magnitude (i.e., small objects). Therefore, we decide to test the percentage of high-amplitude objects for smaller size. We follow the same approach as was previously used, but we now only focus on objects with $H \geqslant 6.0$ mag (diameter of 419/188 mag assuming an albedo of 0.04/0.2). Based on our sample and the literature, we have: $f(\Delta_m \geqslant 0.7\,\mathrm{mag}) \sim 35\%$, $f(\Delta_m \geqslant 0.6\,\mathrm{mag}) \sim 52\%$, and $f(\Delta_m \geqslant 0.5\,\mathrm{mag}) \sim 50\%$ using Equation (1). With Equation (2), we have: $f(\Delta_m \geqslant 0.7\,\mathrm{mag}) \sim 27\%$, $f(\Delta_m \geqslant 0.6\,\mathrm{mag}) \sim 48\%$, and $f(\Delta_m \geqslant 0.5\,\mathrm{mag}) \sim 52\%$. In conclusion, ~40% of the Plutinos and ~50% of the small Plutinos could be contact binaries using a cut-off at $\Delta_m \geqslant 0.5$ mag.

Several studies mentioned that there is an anti-correlation between size and light-curve amplitude (Thirouin et al. 2010; Benecchi & Sheppard 2013; Thirouin 2013). In other words, at smaller sizes (i.e., larger absolute magnitude), the light-curve amplitude is larger, suggesting that the small objects are more elongated and have a more irregular shape. Such a tendency has been reported in all of the dynamical groups of TNOs (Thirouin 2013). Therefore, one may expect that objects reported in this work are likely to be more elongated/deformed; however, their light curves show U-/V-shapes indicative of contact binaries, and therefore the contact binary option is more likely.

4.3. Correlation/Anti-correlation Search

We also search for correlation/anti-correlation between the light-curve amplitude and the rotational period with the orbital elements (technique detailed in Thirouin et al. 2016). Only two strong trends have been identified (Figure 7): the light-curve amplitude is correlated with the absolute magnitude ($\rho = 0.544$, significance level = 98%), and an anti-correlation between light-curve amplitude and inclination ($\rho = -0.505$, significance level = 97%). The correlation between amplitude and size suggesting that the smaller objects present a large variability has been already noticed in several works and seems to be present in all of the TNO dynamical groups (Sheppard et al. 2008; Benecchi & Sheppard 2013; Thirouin 2013). The anti-correlation between amplitude and inclination suggests that the variable objects are at low inclination. Such a trend has been noticed in several sub-populations of TNOs (Thirouin 2013). However, it is interesting that the large-amplitude objects are located at low inclination in the Plutino population. Sheppard (2012) concluded that the 3:2 population presents a large variety of colors from neutral to ultra-red, suggesting a Cold Classical component at low inclination. Unfortunately, we do not have color studies for our objects to identify them as ultra-red objects (i.e., as a Cold Classical TNO) or not. However, color studies are available for 2001 QG_{298} and 2000 GN_{171} (Sheppard & Jewitt 2002, 2004). With a B-R of 1.6 mag for 2001 QG_{298} and 1.55 mag for 2000 GN_{171}, both objects are very red. Typical error bars are ± 0.04 mag, and thus, taking into account this uncertainty, both objects are potentially ultra-red. In conclusion, both objects are potentially presenting characteristics that are similar to the dynamical Cold Classical TNOs. By studying the contact binaries in the Plutino and the Cold Classical populations, one will be able to check if both populations share the same binary fraction and characteristics, if there was some leakage of objects between the two populations, and constrain Neptune's migration (paper in preparation).

5. Conclusions

We have displayed the data of 12 Plutinos over two years using the Lowell's DCT. A homogeneous data set reduced and analyzed the same way is presented. Our findings can be summarized as follows:

1. For nine objects, we report partial light curves showing a typical variability lower than 0.2 mag. Three objects in our sample of 12 are showing a light-curve amplitude larger than 0.5 mag (25% of our sample). 2014 JL_{80} is the slowest rotator in our sample with a period of 34.87 hr and an amplitude of 0.55 mag. The period of 2014 JO_{80} is 6.32 hr and the amplitude is 0.60 mag. In the case of 2014 JQ_{80}, the light-curve amplitude is 0.76 mag and the rotational period is 12.16 hr. Light curves of 2014 JL_{80}, and 2014 JQ_{80} display a U- and V-shape, indicating they are contact binaries. In the case of the very slow rotator 2014 JL_{80}, the V-shape seems to be present, but unfortunately, we do not have the U-shape of the curve in our data.
2. The large amplitudes light curves are best explained by contact binary systems, but single very elongated objects cannot be ruled out. Assuming a contact binary configuration, we derive $q = 0.5$ and a density of 1 g cm^{-3} for 2014 JL_{80}, a $q = 0.3$ and a density of 3.25 g cm^{-3} for 2014 JO_{80}, and $q = 0.6$ with a density of 1 g cm^{-3} for 2014 JQ_{80}.
3. Thanks to this study, the current population of likely/confirmed contact binaries is composed of eight TNOs: one dynamically Cold Classical object (Thirouin & Sheppard 2017), one in the Haumea family (Lacerda et al. 2014), one in the 5:2 mean motion resonance (Thirouin et al. 2017), and five in the Plutino population (this work, and Sheppard & Jewitt 2002, 2004).
4. Based on our sample, we estimate the fraction of contact binaries in the Plutino population. Using a cut-off of 0.5 mag, we find that ~40% of the Plutinos could be contact binaries. Interestingly, all of the known contact binaries in the Plutino population are small, with absolute magnitude $H \geqslant 6$ mag. We estimate a contact binary fraction of about 50% for the small Plutinos. This suggests that the Plutino population may have significantly more contact binaries than other TNO populations. Future observations of smaller objects in other TNO populations are needed to confirm (or disprove) this finding.

The authors thank the anonymous referee for helpful comments and corrections. This research is based on data obtained at the Lowell Observatory's Discovery Channel Telescope (DCT). Lowell operates the DCT in partnership with Boston University, Northern Arizona University, the University of Maryland, and the University of Toledo. Partial support of the DCT was provided by Discovery Communications. LMI was built by Lowell Observatory using funds from the National Science Foundation (AST-1005313). We acknowledge the DCT operators: Andrew Hayslip, Heidi Larson, Teznie Pugh, and Jason Sanborn. A.T. is partly supported by Lowell Observatory. The authors also acknowledge support from the National Science Foundation, and the grant awarded to the "Comprehensive Study of the Most Pristine Objects Known in the Outer Solar System" (AST-1734484).

Appendix

The Appendix comprises Table 4.

Table 4
Photometry Used in This Paper

Object	JD	Rel. mag. (mag)	Err. (mag)
1995 HM_5			
	2457893.81062	0.03	0.04
	2457893.82056	0.00	0.04
	2457893.83067	−0.08	0.01
	2457893.84067	−0.05	0.02
	2457893.85073	−0.04	0.03
	2457893.86061	−0.04	0.01
	2457893.87065	0.00	0.02
	2457893.88050	0.03	0.05
	2457893.89038	0.00	0.03
2001 KB_{77}			
	2457922.69978	0.00	0.03
	2457922.74331	0.00	0.03
	2457922.76815	0.07	0.04
	2457922.83814	0.03	0.03
	2457922.85305	−0.06	0.03
	2457922.86298	−0.08	0.03
2006 UZ_{184}			
	2457356.78287	−0.08	0.05
	2457356.79985	−0.13	0.05
	2457356.81682	−0.07	0.06
	2457356.83377	−0.03	0.06
	2457356.85215	0.03	0.07
	2457356.86895	−0.06	0.07
	2457357.83488	0.09	0.12
	2457357.85205	0.14	0.11
	2457357.86094	0.25	0.12
	2457357.87037	0.24	0.12
2014 JL_{80}			
	2457901.76402	0.14	0.03
	2457901.77899	0.15	0.03
	2457901.79376	0.15	0.03
	2457901.80857	0.14	0.03
	2457901.82354	0.07	0.03
	2457901.83837	0.03	0.03
	2457901.85321	0.01	0.03
	2457901.86809	−0.01	0.03
	2457901.88304	−0.05	0.03
	2457901.89786	−0.02	0.05
	2457902.82155	−0.28	0.03
	2457902.83643	−0.29	0.03
	2457902.85129	−0.30	0.03
	2457902.86610	−0.25	0.03
	2457902.87091	−0.29	0.03
	2457902.88573	−0.23	0.03
	2457902.90052	−0.19	0.03
	2457902.91029	−0.21	0.04
	2457922.68985	0.10	0.03
	2457922.73343	0.24	0.03
	2457922.75813	0.20	0.03
	2457922.78302	0.19	0.03
	2457922.79789	0.17	0.03
	2457922.81280	0.10	0.03
	2457922.82776	0.05	0.03
	2457932.70192	−0.16	0.02
	2457932.71803	−0.13	0.02
	2457932.73411	−0.11	0.02
	2457932.75037	−0.08	0.02
	2457932.77251	0.04	0.03
2014 JK_{80}			
	2457931.71324	0.01	0.03
	2457931.73529	0.11	0.02
	2457931.75585	0.12	0.02
	2457931.86866	−0.03	0.03
	2457932.67154	0.08	0.03
	2457932.69694	0.04	0.02
	2457932.71301	−0.01	0.02
	2457932.72915	−0.03	0.02
	2457932.74536	−0.02	0.02
	2457932.76141	−0.05	0.02
2014 JO_{80}			
	2457922.51572	−0.22	0.04
	2457922.55931	0.04	0.04
	2457922.58397	0.21	0.05
	2457922.60888	0.02	0.05
	2457922.62380	−0.11	0.04
	2457922.63871	−0.10	0.04
	2457922.65367	−0.08	0.04
	2457922.66899	−0.09	0.05
	2457922.67890	−0.02	0.06
	2457922.68883	0.05	0.06
	2457922.69364	−0.03	0.06
	2457922.69845	0.16	0.08
	2457922.70355	0.02	0.07
	2457931.59498	−0.10	0.04
	2457931.61365	−0.06	0.04
	2457931.62604	0.00	0.04
	2457931.67432	0.06	0.06
	2457932.48703	−0.08	0.06
	2457932.51189	−0.08	0.04
	2457932.52791	−0.14	0.03
	2457932.54409	−0.11	0.03
	2457932.56027	0.03	0.03
	2457932.57636	0.20	0.04
	2457932.58742	0.30	0.04
	2457932.59845	0.22	0.04
	2457932.60441	0.17	0.04
	2457932.61036	0.04	0.03
	2457932.61633	−0.07	0.03
	2457932.62227	−0.07	0.03
	2457936.48638	−0.18	0.08
	2457936.49655	0.01	0.09
	2457936.50709	0.10	0.09
	2457936.51822	0.11	0.09
	2457936.52931	0.39	0.10
	2457936.54040	0.13	0.08
	2457936.55159	0.09	0.07
	2457936.56266	0.11	0.07
	2457936.57412	−0.02	0.08
	2457936.58614	−0.13	0.06
	2457936.59847	−0.18	0.06
	2457936.62931	−0.23	0.05
2014 JP_{80}			
	2457931.85879	0.01	0.02
	2457931.87378	0.02	0.02
	2457931.87801	0.00	0.02
	2457931.88222	−0.01	0.02
	2457931.88645	−0.01	0.02
2014 JQ_{80}			
	2457874.56771	0.28	0.05
	2457874.58431	0.26	0.04
	2457874.61256	0.01	0.03

Table 4
(Continued)

Object	JD	Rel. mag. (mag)	Err. (mag)
	2457874.63733	−0.06	0.03
	2457874.64747	−0.12	0.03
	2457874.66268	−0.13	0.03
	2457874.67782	−0.12	0.02
	2457874.68806	−0.14	0.02
	2457874.69826	−0.09	0.03
	2457874.70837	−0.05	0.03
	2457874.71855	−0.01	0.03
	2457874.72859	0.01	0.03
	2457874.73764	0.10	0.03
	2457874.74648	0.21	0.03
	2457893.63097	−0.06	0.03
	2457893.64101	−0.04	0.03
	2457893.65111	−0.10	0.04
	2457893.66115	−0.13	0.03
	2457893.67116	−0.19	0.03
	2457893.68113	−0.21	0.03
	2457893.69109	−0.25	0.03
	2457893.70102	−0.17	0.03
	2457893.71090	−0.17	0.03
	2457893.72083	−0.08	0.04
	2457893.72562	0.00	0.04
	2457893.73051	−0.01	0.04
	2457893.73529	0.00	0.04
	2457893.74010	0.05	0.05
	2457893.74489	0.08	0.04
	2457893.74970	0.07	0.05
	2457893.75449	0.13	0.05
	2457901.48354	−0.02	0.03
	2457901.49326	−0.04	0.03
	2457901.50170	−0.09	0.03
	2457901.51366	−0.08	0.03
	2457901.52225	−0.12	0.03
	2457901.53065	−0.19	0.03
	2457901.53909	−0.10	0.03
	2457901.54762	−0.11	0.03
	2457901.55603	−0.11	0.03
	2457901.56440	−0.08	0.03
	2457901.58213	0.01	0.03
	2457901.59716	0.07	0.03
	2457901.61194	0.27	0.03
	2457901.62676	0.35	0.03
	2457901.64163	0.53	0.04
	2457901.65651	0.51	0.04
	2457901.67137	0.47	0.04
	2457901.68621	0.23	0.03
	2457901.70116	0.09	0.04
	2457901.71594	0.03	0.04
	2457902.63970	0.33	0.04
	2457902.65451	0.45	0.05
	2457902.68421	0.51	0.06
	2457902.70386	0.28	0.05
	2457902.71862	0.21	0.05
	2457902.72843	0.02	0.05
	2457902.73822	−0.06	0.05
	2457902.74311	−0.03	0.05
	2457902.74794	−0.03	0.05
	2457922.50729	−0.17	0.03
	2457922.55085	−0.12	0.03
	2457922.57560	−0.09	0.03
	2457922.60046	0.12	0.04
	2457922.61527	0.13	0.04
	2457922.63021	−0.06	0.03

Table 4
(Continued)

Object	JD	Rel. mag. (mag)	Err. (mag)
	2457922.64512	0.28	0.04
	2457931.51794	0.33	0.11
	2457931.52869	0.74	0.12
	2457931.55075	0.63	0.06
	2457931.56522	0.53	0.04
	2457931.58388	0.44	0.04
	2457931.60254	0.32	0.04
2014 JT_{80}			
	2457931.76831	0.00	0.03
	2457931.78695	−0.10	0.03
	2457931.79933	0.03	0.03
2014 KC_{102}			
	2457922.70464	−0.02	0.03
	2457922.74820	−0.04	0.03
	2457922.77305	−0.01	0.03
	2457936.68128	0.02	0.04
	2457936.70355	−0.06	0.04
	2457936.72572	−0.07	0.03
	2457936.74803	−0.11	0.04
	2457936.77202	−0.01	0.03
	2457936.78435	0.00	0.03
	2457936.78916	0.00	0.03
	2457936.79394	0.00	0.03
	2457936.79875	0.04	0.03
	2457936.80354	0.00	0.03
	2457936.81460	0.03	0.03
	2457936.81941	0.06	0.03
	2457936.83553	0.07	0.03
	2457936.84842	0.05	0.02
	2457936.86129	0.11	0.03
2014 KX_{101}			
	2457901.78398	−0.02	0.03
	2457901.79876	0.01	0.04
	2457901.82852	−0.01	0.04
	2457901.85819	0.16	0.04
	2457901.87313	0.13	0.05
	2457901.88802	0.12	0.05
	2457901.90293	0.10	0.08
	2457901.91350	0.11	0.11
	2457902.82649	−0.02	0.04
	2457902.84142	−0.01	0.04
	2457902.85625	−0.06	0.04
	2457902.87591	−0.10	0.04
	2457902.89068	0.00	0.05
2015 BA_{519}			
	2457874.73348	−0.03	0.04
	2457874.74995	−0.06	0.04
	2457874.76792	−0.08	0.03
	2457874.78450	−0.05	0.04
	2457874.79498	−0.04	0.03
	2457874.79977	−0.03	0.04
	2457874.80458	−0.02	0.04
	2457874.80936	0.00	0.04
	2457874.81954	0.02	0.04
	2457874.83469	0.05	0.04
	2457874.84984	0.08	0.04
	2457874.86009	0.08	0.04
	2457874.87030	0.06	0.04
	2457874.88044	0.03	0.04
	2457874.90070	0.00	0.04

ORCID iDs

Audrey Thirouin https://orcid.org/0000-0002-1506-4248
Scott S. Sheppard https://orcid.org/0000-0003-3145-8682

References

Benecchi, S. D., & Sheppard, S. S. 2013, AJ, 145, 124
Binzel, R. P., Farinella, P., Zappala, V., & Cellino, A. 1989, Asteroids II (Tucson, AZ: Univ. Arizona Press), 416
Bodenheimer, P. H. 2011, Principles of Star Formation (Berlin Heidelberg: Springer)
Brown, M. E. 2001, AJ, 121, 2804
Brown, M. E. 2013, ApJL, 778, L34
Buie, M. W., Tholen, D. J., & Wasserman, L. H. 1997, Icar, 125, 233
Buratti, B. J., Hofgartner, J. D., Hicks, M. D., et al. 2017, Icar, 287, 207
Chandrasekhar, S. 1987, Ellipsoisal Figures of Equilibrium (New York: Dover)
Chiang, E. I., & Jordan, A. B. 2002, AJ, 124, 3430
Collander-Brown, S. J., Fitzsimmons, A., Fletcher, E., Irwin, M. J., & Williams, I. P. 1999, MNRAS, 308, 588
Compère, A., Farrelly, D., Lemaître, A., & Hestroffer, D. 2013, A&A, 558, A4
Davies, J. K., McBride, N., & Green, S. F. 1997, Icar, 125, 61
Degewij, J., Tedesco, E. F., & Zellner, B. 1979, Icar, 40, 364
Dotto, E., Perna, D., Barucci, M. A., et al. 2008, A&A, 490, 829
Elliot, J. L., Kern, S. D., Clancy, K. B., et al. 2005, AJ, 129, 1117
Fernandez, J. A., & Ip, W.-H. 1984, Icar, 58, 109
Galiazzo, M., de la Fuente Marcos, C., de la Fuente Marcos, R., et al. 2016, Ap&SS, 361, 212
Gladman, B., Marsden, B. G., & Vanlaerhoven, C. 2008, in The Solar System Beyond Neptune, ed. M. A. Barucci et al. (Tucson, AZ: Univ. Arizona Press), 43
Gomes, R. S. 2000, AJ, 120, 2695
Grundy, W. M., Benecchi, S. D., Rabinowitz, D. L., et al. 2012, Icar, 220, 74
Howell, S. B. 1989, PASP, 101, 616
Jeans, J. H. 1919, Problems of Cosmogony and Stellar Dynamics (Cambridge: Cambridge Univ. Press)
Jewitt, D., Luu, J., & Trujillo, C. 1998, AJ, 115, 2125
Lacerda, P. 2011, AJ, 142, 90
Lacerda, P., & Jewitt, D. C. 2007, AJ, 133, 1393
Lacerda, P., & Luu, J. 2006, AJ, 131, 2314
Lacerda, P., McNeill, A., & Peixinho, N. 2014, MNRAS, 437, 3824
Leone, G., Paolicchi, P., Farinella, P., & Zappala, V. 1984, A&A, 140, 265
Levine, S. E., Bida, T. A., Chylek, T., et al. 2012, Proc. SPIE, 8444, 844419
Levison, H. F., Morbidelli, A., Van Laerhoven, C., Gomes, R., & Tsiganis, K. 2008, Icar, 196, 258
Levison, H. F., & Stern, S. A. 2001, AJ, 121, 1730
Lomb, N. R. 1976, Ap&SS, 39, 447
Malhotra, R. 1993, Natur, 365, 819
Malhotra, R. 1995, AJ, 110, 420
Nesvorný, D., Youdin, A. N., & Richardson, D. C. 2010, AJ, 140, 785
Noll, K. S., Grundy, W. M., Chiang, E. I., Margot, J.-L., & Kern, S. D. 2008, in The Solar System Beyond Neptune, ed. M. A. Barucci (Tucson, AZ: Univ. Arizona Press), 345
Ortiz, J. L., Gutiérrez, P. J., Casanova, V., & Sota, A. 2003, A&A, 407, 1149
Ortiz, J. L., Gutiérrez, P. J., Santos-Sanz, P., Casanova, V., & Sota, A. 2006, A&A, 447, 1131
Peixinho, N., Lacerda, P., & Jewitt, D. 2008, AJ, 136, 1837
Perna, D., Dotto, E., Barucci, M. A., et al. 2009, A&A, 508, 451
Porter, S. B., & Grundy, W. M. 2012, Icar, 220, 947
Porter, S. B., Spencer, J. R., Benecchi, S., et al. 2016, ApJL, 828, L15
Press, W. H., Teukolsky, S. A., Vetterling, W. T., & Flannery, B. P. 1992, Numerical Recipes in FORTRAN: The Art of Scientific Computing (2nd ed.; Cambridge: Cambridge Univ. Press)
Rabinowitz, D., Schwamb, M. E., Hadjiyska, E., Tourtellotte, S., & Rojo, P. 2013, AJ, 146, 17
Rabinowitz, D. L., Schaefer, B. E., & Tourtellotte, S. W. 2007, AJ, 133, 26
Romanishin, W., & Tegler, S. C. 1999, Natur, 398, 129
Rousselot, P., & Petit, J. 2010, in AAS/DPS Meeting 42 Abstracts, 40.19
Schaefer, B. E., & Rabinowitz, D. L. 2002, Icar, 160, 52
Sheppard, S. S. 2004, PhD thesis, Univ. Hawaii
Sheppard, S. S. 2007, AJ, 134, 787
Sheppard, S. S. 2012, AJ, 144, 169
Sheppard, S. S., & Jewitt, D. 2004, AJ, 127, 3023
Sheppard, S. S., & Jewitt, D. C. 2002, AJ, 124, 1757
Sheppard, S. S., & Jewitt, D. C. 2003, EM&P, 92, 207
Sheppard, S. S., Lacerda, P., & Ortiz, J. L. 2008, in The Solar System Beyond Neptune, ed. M. A. Barucci et al. (Tucson, AZ: Univ. Arizona Press), 129
Sheppard, S. S., Ragozzine, D., & Trujillo, C. 2012, AJ, 143, 58
Smith, J. A., Tucker, D. L., Kent, S., et al. 2002, AJ, 123, 2121
Snodgrass, C., Carry, B., Dumas, C., & Hainaut, O. 2010, A&A, 511, A72
Stellingwerf, R. F. 1978, ApJ, 224, 953
Stetson, P. B. 1987, PASP, 99, 191
Stetson, P. B. 1990, PASP, 102, 932
Tegler, S. C., Romanishin, W., Stone, A., et al. 1997, AJ, 114, 1230
Thirouin, A. 2013, PhD thesis, Univ. Granada
Thirouin, A., Noll, K. S., Ortiz, J. L., & Morales, N. 2014, A&A, 569, A3
Thirouin, A., Ortiz, J. L., Campo-Bagatin, A., et al. 2012, MNRAS, 424, 3156
Thirouin, A., Ortiz, J. L., Duffard, R., et al. 2010, A&A, 522, A93
Thirouin, A., & Sheppard, S. S. 2017, AJ, 154, 241
Thirouin, A., Sheppard, S. S., Noll, K. S., et al. 2016, AJ, 151, 148
Thirouin, A., Sheppard, S. S., & Noll, K. S. 2017, ApJ, 844, 135
Trilling, D. E., & Bernstein, G. M. 2006, AJ, 131, 1149
Vilenius, E., Kiss, C., Müller, T., et al. 2014, A&A, 564, A35
Weidenschilling, S. J. 1980, Icar, 44, 80
Williams, I. P., O'Ceallaigh, D. P., Fitzsimmons, A., & Marsden, B. G. 1995, Icar, 116, 180